OSL chronology of socio-ecological systems during the mid-Holocene in the eastern coast of the Sultanate of Oman (Arabian Peninsula)

Maïlys Richard, Norbert Mercier, Vincent Charpentier, Jean-François Berger

OSL chronology of socio-ecological systems during the mid-Holocene in the eastern coast of the Sultanate of Oman (Arabian Peninsula)

Richard M.[1], Mercier N.[1], V. Charpentier[2], Berger J.-F.[3]

[1] Institut de Recherche sur les Archéomatériaux - Centre de Recherche en Physique Appliquée à l'Archéologie, UMR 5060 CNRS, Université Bordeaux-Montaigne, 33607 Pessac, France

[2] Institut national de recherches archéologiques préventives, ARSCAN, UMR 7041 CNRS, Université Paris X, 92023 Nanterre, France

[3] CNRS, Environnement Ville Société - Institut de Recherches Géographiques, UMR 5600 CNRS, Université de Lyon, 69676 BRON, France

Abstract

The eastern coast of the Arabian Peninsula is a key region to explore past climatic and environmental changes and their impact on the coastal ecosystems and Neolithic communities during the mid-Holocene (~8000-5000 years ago). Indeed, it is located at the frontier zone between dry and wet tropical systems, where the monsoon has reduced its activity and gradually shifted southward from the 6th millennium BC. Past human adaptation to new ecological conditions (more arid) and resources is reflected in the archaeological record, as a response to important climatic and eustatic fluctuations.

In order to correlate human occupation during the Neolithic with the local climatic and palaeoenvironmental records, sediments were sampled at two archaeological sites and surrounding sabkhas, located in the Ja'alan region, on the eastern coast of the Sultanate of Oman. Optically and infrared stimulated luminescence dating were applied to quartz and feldspar grains extracted from sediments coming from both archaeological (Ruways 1 and Suwayh 1 shell middens) and palaeoenvironmental (current sabkhas) contexts in order to provide, together with radiocarbon dating, a chronology for this area. The results obtained allowed constraining human occupation during the Neolithic between 8340 ± 480 and 5390 ± 290 years (~6800-3100 years BC) at Ruways 1, and between 6180 ± 310 and 5480 ± 270 years BP (~4500-3200 years BC) at Suwayh 1. These occupations coincide with the development of a lagoon/mangrove, recorded in sediments from cores drilled under the

current sabkha, whose last stage of development is dated to 5320 ± 590 (C2) and 5220 ± 570 (C1) years (3900-2600 years BC) at Khor al Jaramah.

1. Introduction

The study of past groups of coastal fisher-gatherer-herders in their palaeoenvironmental context is of great interest to understand the resilience of these populations facing important climatic changes during the mid-Holocene in the Arabian Peninsula. The eastern coast of the Arabian Peninsula, and more specifically the Ja'alan region in the Sultanate of Oman (Fig. 1), presents several important archaeological sites documenting human occupation starting from the middle of the 6th millennium BC (~8000-7000 years; Charpentier 2008; Berger et al., 2005). During the mid-Holocene, this territory suffered climatic (Indian-Arabian monsoon), eustatic and tectonic fluctuations, which might have directly affected Neolithic populations that exploited marine, lagoon and deltaic resources (Berger et al., 2005; Berger et al., 2013).

More specifically, along the Oman coast, a particular Neolithic economy flourished during the first half of the mid-Holocene, without pottery and agriculture but with a significant component of marine resources associated with the presence of a few domesticated animals (Crassard and Dreschler, 2013). Coastal environments and marine resources have played a major role in the Neolithic development of eastern Arabia, as an apparent resilience to climatic variations during the mid-Holocene. After the onset of the humid period around 9000 years (end of the early Holocene), this sub-arid to arid zone suffered rapidly changing environmental conditions, with past latitudinal monsoon circulation and upwelling activity changes through time (Jung et al., 2004, Fleitmann et al., 2007, Parker et al., 2008) that impacted coastal paleoenvironments and biomass productivity (Lézine et al. 2010; Berger et al. 2013; Bassinot et al. 2011).

The effect of climate change on Neolithic populations over a long time, inducing environmental and economic stress, can be investigated by cross-checking data from human occupation in shell middens with palaeoenvironmental records. The evolution of coastal environments can be reconstructed through the study of transects in sections and cores in archaeological sites and surrounding sabkhas. This study focuses on establishing the chronology of the occupation phases of stratified shell middens that were produced by the interaction of aeolian and anthropogenic processes (Ruways 1 and Suwayh 1 archaeological sites), and the chronology of coastal environmental archives that are preserved under the

current surrounding sabkhas (core drilling), with the goal of studying past human behaviour in its palaeoenvironmental context.

2. Archaeological and palaeoenvironmental contexts

Ruways 1 (RWY-1) and Suwayh 1 (SWY-1) (governorate of al-Sharqquiyah, Oman) are located along the coast of the Arabian sea, in a vast plain comprised of sabkhas, which are seasonally fed by wadis coming from large quaternary alluvial fans at the bottom of the Jebel Khamis (Fig. 1). RWY-1 is a site featuring a long sequence of occupations (dated by radiocarbon between 6380 and 3400 years BC) with one potentially dating to the beginning of the middle Neolithic, which is remarkable in a stratified context in Ja'alan (Berger et al., 2020). The RWY-1 and SWY-1 sites present great potential for reconstructing the economic strategies of Neolithic coastal populations, strongly oriented towards the exploitation of lagoons and mangrove ecosystems (Martin, 2005; Berger et al., 2020).

Under the current sabkhas, preserved palaeo-mangroves and lagoons seem to be correlated with mid-Holocene fossil deltas and estuaries. Episodes of marine transgression alternated with mangrove and/or lagoon phases are recorded in stratigraphic profiles at the Suwayh sabkha (Berger et al., 2005). In particular, during the 5th millennium BC (around 7000-6000 years), Neolithic sites are associated to an optimum period for mangrove development, due to sea-level stability (Berger et al., 2013). Around 5000-4500 years, an arid period led to the expansion of sabkhas and the regression of mangroves (Berger et al., 2013). This climatic setting may have affected both settlement networks and economic strategies of the Neolithic populations that occupied the area. To investigate the impact of such environmental and climatic changes on past human populations, cores were drilled at the nearby modern sabkhas of Ruways, Daffah and Khor al Jaramah (Fig. 1). Palaeoenvironmental and climatic data extracted from these cores were used to reconstruct the landscape at the time of occupation of the Ruways 1 and Suwayh 1 shell middens.

2.1. Ruways 1 and Suways 1 shell middens

Ruways 1 (RWY-1) is located at the center of a wide, open and flat coastline of the Arabian Sea. Oriented NE–SW, this coastline associates wadi estuaries with vast sabkhas, where barchanoid dunes were deposited after the disappearance of the mid-Holocene coastal lagoon and mangrove systems. The current system shows peri-desert arid conditions since the increasing aridification of the Late Holocene. The archaeological site extends over 8 hectares and was discovered in 1996 by Mauro Cremaschi (University of Milan) and later prospected

by a French expedition. Ruways 1 was used as a ballast quarry at the beginning of 2010, leading to the destruction of half of the site but revealing continuous, semi-circular stratigraphic sections over nearly 80 m in length and 3 m in height in the eastern part of the shell midden.

Ten sedimentary units were identified in the sequence. At the base, cemented gravels from fluvial-deltaic origin provide the substrate upon which lies the shell midden. Sediment deposition follows vertical and lateral aggradation phases. Erosion caused by aeolian processes was identified throughout the section in the form of truncations of some of the older anthropogenic deposits (Fig. 2). According to two radiocarbon dates obtained on charcoal and marine shells, the settlement started during the late centuries of the 7th millennium BC (around 8300 years BP; Berger et al., 2020). At the surface, archaeological remains indicate an occupation until the 4th millennium BC (around 6000-5000 years, Berger et al., 2020). Besides providing information on the subsistence strategy and technological behaviour of the population, this site contains burials from the Middle Neolithic period that document funeral rituals and periods of stress recorded in human skeletons. Both lithic and shell technology have been used to manufacture stone tools, beads, net sinkers and hooks (Berger et al., 2020). The recovered faunal remains belonged to vertebrates and molluscs, indicating the use of terrestrial, marine and lagoon/mangrove food resources. Among the species identified, mammalian remains can be attributed to sheep and goat, while reptile and turtle remains have also been recovered (Berger et al., 2020). Among the marine shells, the clam *Marcia recens* is the most abundant and indicates that Neolithic populations exploited species from the silty-sand of the lagoon. Most of the fish remains were attributed to species living in brackish waters, such as mullet (*Mugilidae*), sardine (Clupeiformes) and sea bream (*Sparidae*). These species, along with catfish (*Ariidae*), indicate the occurrence of a paleo-lagoon and a mangrove in the vicinity of Ruways 1 which were preferentially exploited by the Neolithic populations (Berger et al., 2020). Botanical macro-remains also allow reconstructing the local environment. *Avicennia marina* is the dominant species identified among the charred wood in the upper part of the sequence with, to a lesser extent, *Rhizophora cf mucronata* attesting the existence of a mangrove, today absent. Semi-desert taxa such as *Chenopodiaceae* were also documented (Berger et al., 2020).

Suwayh 1 (SWY-1) is a Neolithic shell midden covering ca. 25,000 m² of surface area. It is located along an old wadi estuary, between modern sabkhas and the Arabian Sea (Fig. 1). Similar to Ruways 1, the site was partially destroyed when it was used as a ballast quarry 20 years ago. The excavations conducted during the 2000's allowed documenting a stratigraphic

sequence of 2 m thick (Fig. 3), with human occupation levels from the 6th and 5th millennia (~8000-6000 years BP) and a necropolis in the recent portion of the site (Charpentier, et al. 2003). Seven test pits were opened for documenting the phases of the occupation. Unlike the tombs, these levels are rich in archaeological material, mainly comprised of fishing instruments such as stone net sinkers, shellfish hooks and jewellery. Dwellings were uncovered in different phases of the site (Charpentier et al., forthcoming). SWY-1 is dated to the Middle Neolithic period (Charpentier, 2008) and is a settlement specialised in shark fishing (Marrast et al., 2020). The palaeoecological data available for this site indicate that, starting from ~6500 years ago (~4500 years BC), species from mangroves (e.g., *Terebralia palustris*) are represented and preceded species collected from the lagoon environment (*Amiantis umbonella*) (Martin 2005, Berger et al., 2005).

The sedimentation rate of these two shell middens is highly variable and depends on the rate of aeolian sedimentation (and truncation events) and anthropogenic deposition. It is primarily the human accumulation of shells and rocks/pebbles that allowed the construction of these coastal sedimentary anomalies. They favour the trapping of sand particles during human occupation and protect it afterwards. The lithostratigraphic and sedimentological study has revealed sets of sedimentary units that are clearly aeolian (facies with more or less pure allogenic sand) or clearly anthropogenic (facies rich in ash, charcoal, accumulations of shells or fish bones linked to past human occupations) and intermediate facies, revealing the more or less strong reworking of anthropogenic deposits by aeolian processes (Berger et al. 2020). Sedimentological, magnetic and geochemical analyses are ongoing.

2.3. Cores

In 2017 and 2018, a systematic off-site geoarchaeological and geophysical survey was performed across the modern sabkhas, associated with electrical resistivity tomography (ERT) measurements and thermic mechanical coring to depths up to 3-5 m (with a Cobra corer). Three cores were drilled in the following localities: Ruways, Daffah and Khor al Jaramah (Fig. 1). Sedimentological data extracted from the cores were used to reconstruct the middle Holocene landscape: they indicate that the lagoons and mangroves were located under the modern sabkhas.

Four main sedimentary units were distinguished in the upper 10 m: 1) at the base, a deep and probably late Quaternary alluvial formation (not reached by cores); 2) coarse sandy to gravelly alluvial pre-mid-Holocene deposits organised in a succession of paleochannels; 3)

fine fluvial-lagoon silty-sand formations associated with the maximum marine transgression, 4) red silts and gypsum interbedded with aeolian sands corresponding to the current sabkha (Berger et al. 2020). OSL dating was carried out on this latter sedimentary unit (upper part of the core), allowing to date the latest episode of lagoon/mangrove development.

3. Materials and Methods

3.1. Sampling and preparation

Sediment samples (n = 21) were collected at different localities (Ruways, RWY, Suwayh, SWR, Daffah, DAF and Khor al Jaramah, KAJ; Tab. 1) during the 2017 expedition (SOM Figs. S1 to S13). For the archaeological sites, sediments were mostly sampled using lightproof bags during the night after cleaning the section to avoid any contamination by newly bleached grains. Regarding the cores, sediments were sampled using a lightproof tube that was inserted either in the section of the test pit dug near the core (Ruways and Daffah, SOM Figs. S10 and S11) or directly in the core (Khor al Jaramah; SOM Figs. S12 and S13). For Ruways 1, sediments were sampled from the base to the top of the sequence (phases I, II, VII, VIII and IX, SOM Figs. S1 to S8); for Suwayh 1, only the upper levels were sampled from a test pit (SOM Figs. S9); for the cores, sampling was focused on the lagoon/mangrove levels.

Sample preparation and OSL measurements were conducted at the IRAMAT-CRP2A (Institut de Recherche sur les Archéomatériaux-Centre de Recherche en Physique Appliquée à l'Archéologie) at Bordeaux Montaigne University. Wet sieving was performed to extract the most abundant granulometric fraction, 100-120, 120-160 or 160-200 µm depending on the sample (Tab. 1). Chemical treatment included HCl (10%) to dissolve carbonates and H_2O_2 (30%) to break down organic matter. Feldspars were dissolved using H_2SiF_6 (31%) over one week. Finally, quartz grains were rinsed with HCl (10%) and sieved again (using 100, 120 or 160 µm sieves for the 100-120, 120-160 or 160-200 µm granulometric fractions, respectively) to eliminate partially dissolved feldspar grains.

3.2. Equivalent dose determination

Equivalent doses (D_e) were determined by applying the single aliquot regeneration (SAR) protocol (Murray and Wintle, 2000) to multi-grain aliquots (1 mm ø) analysed with a lexsyg SMART TL/OSL reader (Richter et al., 2015) for the quartz samples, and with a lexsyg research TL/OSL reader (Richter et al., 2013) for the feldspar samples. D_e values were

obtained on quartz using the protocol described in Tab. 2. For BDX 19229, whose signal reached saturation, and for BDX 19235, $pIRIR_{225}$ measurements were performed (Tab. 3).

Regarding the measurement procedure, green LEDs were used for stimulation (stimulation power density of 50 $mW \cdot cm^{-2}$) and the OSL signal was detected with a combination of UV filters (Schott BG-3, 3 mm in conjunction with a Delta BP365/50 EX). Aliquots were irradiated using the inbuilt $^{90}Sr/^{90}Y$ beta-sources fitted to the readers. An infrared stimulation at 50°C for 60 s was performed before each OSL measurement to avoid potential contamination from remaining feldspars. We observed a dominant fast decaying OSL signal component for our quartz samples (Fig. 4).

For BDX19229 and BDX19235, the $pIRIR_{225}$ protocol (Thomsen et al., 2008; Buylaert et al., 2011) was applied (Tab. 3). Infrared laser diodes were used for stimulation (power density: 120 $mW \cdot cm^{-2}$) and the signal was detected with a combination of optical filters (Schott KG3, 3 mm + Chroma D410/30 x for the research reader).

Preheat plateau tests were conducted on natural aliquots from samples BDX 19231 and 19232 (Ruways 1) and BDX 19238, 19239 and 19240 (Suwayh 1). For Ruways 1 samples, measurements were done between 180°C and 300°C (cutheat = 200°C) with 20°C steps; for Suwayh 1 samples, from 170°C to 250°C (cutheat = 160°C) with 20°C steps. Since low D_e values were observed after preliminary tests, the preheat temperature tests were conducted on lower temperatures for Suwayh 1 samples.

Dose recovery tests (DRT) were performed on each sample, on three to five bleached aliquots (n = 74; Tab. 4), using the preheat and cutheat temperatures mentioned above. The aliquots were bleached in a solar simulator (Hölne SOL500) for 1 min. The irradiation dose applied was similar to the one expected on natural aliquot.

All data were processed using the software Analyst v.4.52 (Duller, 2007). The signal was integrated using the first 1.5 s for quartz and the first 5 s for feldspars, while the background was subtracted from the last 15 s for quartz and the last 30 s for feldspars. The following criteria were applied for D_e values selection: a recycling ratio limit of 10%; a maximum recuperation of 5% of the natural signal; a test dose signal more than 3 sigma above background. Equivalent doses were obtained by fitting an exponential function through the normalised luminescence signals. The statistic treatment of the D_e values was done using either the Central Age Model (CAM, Galbraith et al., 1999) or the Finite Mixture Model (FMM, Galbraith and Green, 1990) for samples exhibiting a large scatter of the D_e values.

3.3. Dose rate determination

3.3.1. Alpha and beta dose rates

A portion of the sediment sampled from the section or the core (see Tab. 1) was dried in an oven for one week at 40 °C and the water content (wet weight %) measured. ^{238}U, ^{232}Th and K contents were determined using a laboratory gamma-ray spectrometer equipped with a high-resolution, broad energy Ge (BEGe) detector. Since no HF treatment was applied, both alpha and beta dose rates were derived from these values taking into account the conversion factors of Guérin et al. (2011).

3.3.2. Gamma dose rate

For all samples except those collected directly from the KAJ core (BDX 19245 and 19246; SOM Figs. S12 and S13) and for samples BDX 19232 and 19237 from Ruways 1, whose location did not allow to safely dig a 30 cm deep hole in the section (SOM Figs. S4 and S8), the gamma dose rate was measured *in situ* using a portable gamma-ray multichannel analyser connected to a NaI(Tl) detector. The data were processed following the "threshold" technique (Mercier and Falguères, 2007). For the other samples, the gamma dose rate was derived from their ^{238}U, ^{232}Th and K contents deduced from BEGe gamma spectrometric analyses.

3.3.3. Cosmic dose rate

The depth of the sampling position was measured from the surface level (Tab. 1). This value was used to calculate the cosmic dose rate according to Prescott and Hutton (1988).

4. Results

OSL ages on quartz and $pIRIR_{225}$ ages on feldspar aliquots were calculated with the 1 σ error range, taking into account the alpha attenuation and beta absorption factors of Brennan et al. (1991) and Guérin et al. (2012) respectively. Water content values used for age calculation range from 3% to 27% depending on the context (measured values, Tab. 5).

4.1. Equivalent doses

4.1.1. Preheat plateau test

Results obtained do not show temperature dependence between 180°C and 280°C for Ruways 1 samples (SOM Fig. S14), and between 170°C and 250°C for Suwayh 1 samples (SOM Fig. S15). Measurements were thus conducted using a 260°C preheat temperature and 200°C cutheat temperatures for Ruways 1 samples, and using lower temperatures for Suwayh 1 (210°C preheat; 160°C cutheat) and cores samples (190°C preheat; 160°C cutheat).

4.1.2. Dose recovery tests

For Ruways 1 and Suwayh 1 samples, dose recovery ratios range from 0.96 ± 0.03 to 1.04 ± 0.05 (Tab. 4). For the core samples, dose recovery ratios are close to 1 except for BDX 19243 (Daffah C2) that yields a higher recovery ratio of 1.44 ± 0.16. This high value can be related to the low irradiation dose applied (0.5 Gy), which is similar to the natural dose, and to a relatively high residual signal after bleaching.

4.2. Interpreting D_e values distribution

The distribution of D_e values is heterogeneous for most of the samples (Tab. 6), as shown in Fig. 5 (Ruways 1 phase II). Indeed, when applying the Central Age Model (CAM, Galbraith et al., 1999), overdispersion (OD) values are higher than 20% for half of the samples, and 5 out of 21 D_e values have OD >50% (Tab. S1). This indicates that several grain populations are present, which may result from differential bleaching and/or microdosimetry effects. The superposition of these populations can be described using the finite mixture model (FMM, Galbraith and Green, 1990). However, this model must be applied with caution on data obtained from the analysis of multi-grain aliquots because averaging effects may occur, even for small aliquots (Arnold and Roberts, 2009; Galbraith and Roberts, 2012). However, considering that only a small percentage of grains give rise to the OSL signal (typically ~5% produce 95% of the total light sum, Duller et al. (2000)), the FMM model is applicable when only a few grains have been measured, which is the case here with our 1 mm ø aliquots (e.g., Preusser et al., 2011). FMM modelling was thus conducted for samples with a number of measured aliquots (n) $\geq$ 22 and OD >15% (a sigma-b value of 0.10 was assumed) ; the components (central value and proportion) are presented in Tab. S2. For samples with n aliquots < 22, only the CAM was applied, including the feldspar samples from Ruways 1 (BDX 19229 and 19235) and some of the quartz samples from the cores (BDX 19242, 19244, 19245 and 19246) (Tab. 6). For $pIRIR_{225}$ ages, no residual dose nor fading corrections were applied. However, considering that the IRSL age for BDX 19235 is in agreement with OSL ages obtained for Phase II (BDX 19226, 19227, 19228 and 19236, Tab. 6), the effect of these two variables might have been compensated for this sample.

D_e values obtained either using the FMM or CAM model are presented in Tab. 6 and Tab. S1. FMM D_e values are systematically lower than CAM D_e values, but considering the associated uncertainties, most of the values are indistinguishable (Fig. 6). Nevertheless, the use of the main FMM component (Tab. S2) help to discard incomplete bleached grains which,

when taken into account (as it is the case with the CAM model), induce an overestimation of the mean D_e values.

For Ruways 1, CAM D_e values range from 0.29 ± 0.05 to 8.55 ± 0.53 Gy for the quartz samples and from 14.78 ± 1.55 to 520.66 ± 79.78 Gy for the feldspar samples, with OD values between 9 ± 2 and 98 ± 13 %. FMM D_e values range from 0.13 ± 0.01 to 8.12 ± 0.17 Gy for the quartz samples.

For Suwayh 1, D_e values range from 5.91 ± 0.13 to 7.43 ± 0.25 using the CAM (OD values between 13 ± 2 and 20 ± 2 %). The D_e distribution is thus more homogeneous for these samples in comparison with most of the samples collected in a similar context at Ruways 1. Indeed, some aliquots likely include partially bleached grains, especially BDX 19238 and 19240 (Fig. 7) and the use of the FMM allowed to extract the main D_e component whose proportion represents ≥ 89% (Tab. S2). The resulting D_e values range from 5.76 ± 0.15 to 7.08 ± 0.15 Gy.

For the cores, CAM D_e values vary from 1.68 ± 0.51 to 5.39 ± 0.44 Gy (5.01 ± 0.26 Gy for the FMM) for Ruways-C1, from 0.57 ± 0.06 to 0.70 ± 0.08 Gy (0.66 ± 0.06 Gy for the FMM) for Daffah-C2 and equal 7.92 ± 0.43 and 8.46 ± 0.38 Gy for the Khor al Jaramah-C1 and C2 samples. Consequently, these values indicate either a large range of dose rates or ages significantly different for similar contexts.

4.3. Dose rates

The main contribution to the dose rate comes from the beta dose rate, except for the feldspar samples (Fig. 8). Alpha dose rates were taken into account for all samples since the grains have not been etched. They are low and represent maximum 3% of the total dose rate. Both were derived from ^{238}U, ^{232}Th and K contents of the sediment samples (Tab. 5). For Ruways 1, the ^{238}U content ranges from 0.53 ± 0.01 to 3.20 ± 0.04 ppm and for 7 out of 12 samples, the ^{232}Th content is lower, ranging from 0.57 ± 0.02 to 4.62 ± 0.04 ppm. These low ^{232}Th values for the Ruways 1 sediments are not well understood and further investigations are required to explain the mechanisms. For the Suwayh 1, Ruways-C1, Daffah-C2 and Khor al Jaramah-C1/C2 samples, the ^{232}Th content is systematically higher than ^{238}U content. K contents vary also considerably, ranging from 0.16 ± 0.01 (RWY, BDX 19226) to 1.26 ± 0.02 (KAJ-C2, BDX 19246). The highest K contents were measured in the core samples where the sediments were essentially composed of clayey silt.

The gamma dose rate was measured *in situ* for most of the samples (Tab. 6). In-situ measurements values range from 210 ± 10 to 405 ± 20 $\mu Gy.a^{-1}$ for Ruways 1, from 207 ± 10

to 345 ± 17 µGy.a^{-1} for Suwayh 1, from 331 ± 17 to 372 ± 19 µGy.a^{-1} for Daffah-C1/C2 and overlap for Ruways-C1 (475 ± 24 to 478 ± 24 µGy.a^{-1}). The gamma dose rates calculated for BDX 19232 and 19237 using the U, Th and K contents (444 ± 3 and 276 ± 2 µGy.a^{-1}), fall within the same range than those measured *in situ*. For Khor al Jaramah samples, the gamma doses derived from radioelements contents (481 ± 6 and 494 ± 4 µGy.a^{-1}) are similar to those measured using the portable gamma-probe at Ruways-C1 (around 475 µGy.a^{-1}); this is in agreement with the environmental dose rates that were not measured *in situ* for these samples (SOM Figs. S11 and S12).

For the feldspar samples, a value of 10 ± 1% was taken into account for the internal K content of the feldspar grains. The associated internal dose rate, of 500 ± 50 µGy.a^{-1}, represents up to 42% of the dose rate (Fig. 8), thus being an important parameter for the age calculation.

The cosmic dose was calculated considering the present thickness of sediments, then leading to minimum values. They represent between 14% and 27% of the total dose rate (Fig. 8). However, for the top of the sequence at Ruways 1 (< 60 cm from the top of the section), human occupation is less frequent and erosion/reworking processes by deflation (sandstorm) may have occurred, impacting the cosmic dose rate that can therefore not be estimated with precision.

5. Age interpretation and discussion

FMM ages were used for age interpretation for samples with OD values ≥ 15% and *n* aliquots measured ≥ 22 aliquots. Indeed, for these samples, CAM D_e values appear overestimated likely due to the presence of partially bleached grains (Tab. S3). CAM ages were used for interpretation for samples with OD values < 15% and/or *n* aliquots measured < 22 aliquots.

Ages obtained for the archaeological sequence of the Ruways 1 shell midden range from 440 ± 76 ka to 100 ± 10 years, indicating a deposition time from the Middle Pleistocene to the late Holocene (Tab. 6 and Fig. 9). Phase I, corresponding to a gravelly substrate, deposited by a river, is dated to 440 ± 76 ka using $pIRIR_{225}$. Phase II, corresponding to the first Neolithic occupation, is dated between 8340 ± 480 and 7740 ± 580 years (6800-5200 years BC). A weighted mean age of 7930 ± 240 years is obtained for this unit. Phases VII and VIII are characterised by aeolian sand sedimentary structures where deflation forms predominate. Phase VII is dated to 5930 ± 370 years (4280-3540 years BC) and phase VIII,

from 5830 ± 320 to 5390 ± 290 years (3100-4100 years BC). For this phase, OD values are low (9-13%) indicating that quartz grains were well bleached before deposition and leading to indistinguishable CAM and FMM ages. Finally, ages obtained for phase IX, composed of sediment that fills a deflation corridor interlocking phase VI, range from 3410 ± 190 to 100 ± 10 years. They indicate that the sediment at the top of the sequence was disturbed, which led to a recent resetting of the OSL signal. The age of 3410 ± 190 years should thus be considered as a minimum age, the two other samples from this unit being dated to around 250 and 100 years. Consequently, human occupation at Ruways 1 spans the mid-Holocene: OSL ages indicate a deposition time from the 6th millennium BC (phase II) to the 4th millennium BC (phase VIII), with the main occupation occurring during the 4th millennium BC (phases VII and VIII).

At Suwayh 1, age results range from 6180 ± 310 to 5480 ± 270 years (4500-3200 years BC) and are contemporaneous with phases VII and VIII at Ruways 1. However, OSL ages tend to be slightly younger than radiocarbon ages obtained on shells, by 500-700 years (calibrated with a Δ=0, Marrast et al., 2020; Charpentier et al., forthcoming). Two hypotheses could explain this phenomenon: ^{14}C ages might be overestimated due to the reservoir effect that is not well constrained in the region, and/or OSL ages are underestimated because of the post-burial increase in U in the sediments caused by the proximity to the mouth of the wadi.

With regard to the cores, ages range from 3110 ± 370 to 970 ± 290 years for Ruways-C1, from 540 ± 70 to 420 ± 50 years for Daffah-C2 and are 5220 ± 570 and 5320 ± 590 years for Khor al Jaramah-C1 and C2, respectively. These age results indicate that the top of the Ruways-C1 and Daffah-C2 cores are recent deposits that cannot be correlated with the occupations at the shell middens. Indeed, these deposits belong to the post-Neolithic hyper-arid phase. However, the ages for BDX 19245 and 19246 (Khor al Jaramah-C1 and C2) indicate that a phase of lagoon/mangrove development occurred ~5900-4600 years ago (3900-2600 years BC) and are contemporaneous with human occupation at Ruways 1 (phases VII/VIII) and Suwayh 1 (Fig. 9). Considering the depth of the sampling (90-100 cm) and that earlier paleolagoon episodes were identified in a 480 cm-deep core drilled in Ruways (core 4) and dated using ^{14}C on shells from ~6700 years BP (5000-5400 years BC) (Berger et al., 2020), the dates obtained at Khor al Jaramah could be related to the end of the lagoon/mangrove development.

Previous palynological and micropalaeontological analyses and ^{14}C ages on shells obtained from cores drilled under the modern sabkhas at Suwayh indicate that an optimum period for mangrove development occurred ~6000 years ago (Lézine et al., 2002). This

episode was followed by two phases of seawater incursion ca. 5100 and 4500 years ago that led to the formation of a lagoon (Lézine et al., 2002). Based on geological and environmental data from the Suwayh and Alashkara sabkhas, Berger et al. (2005, 2013) highlighted at least five sea-level transgressions that occurred between ~6800-6400 and ~4400-4200 years ago. The resolution of the OSL ages obtained in this study does not allow to correlate the lagoon episodes recorded in the studied cores with a specific phase. However, both palaeoenvironmental and palaeoclimatic data extracted from the Khor al Jaramah cores can be correlated with human occupation phases at Ruways 1 and Suwayh 1, based on our chronological data.

6. Conclusions

Luminescence dating (OSL and $pIRIR_{225}$) was performed on sediment sampled from both archaeological and geological contexts, in order to correlate human occupation at Ruways 1 and Suwayh 1 shell middens with palaeoclimatic and palaeoenvironmental data preserved in sediments under the modern sabkhas at Ruways, Daffah and Khor al Jaramah. This work aimed at establishing the timeline of Neolithic occupation phases at the two shell middens, as well as providing a chronology for lagoon/mangrove phases that are linked to sea level variations and important climate change during the mid-Holocene.

For most of the samples, the large scatter of the D_e values suggested the presence of several grain populations characterised by different levels of bleaching at the time of deposition, and/or submitted to different dose rates (microdosimetry heterogeneities). For such samples, the FMM model was applied and the D_e values were compared with those calculated using the CAM model. The ages are in agreement with the general stratigraphic order, allowing the establishment of an OSL chronology for the Holocene levels, especially for levels with few or no organic remains that can be dated using ^{14}C.

Age results obtained in this study allowed dating human occupation at Ruways 1 from 8340 ± 480 (6320 ± 480 years BC) for the phase II to 5390 ± 290 years (3370 ± 290 years BC) for the phase VIII, and confirm the antiquity of the settlement, as suggested by ^{14}C ages (6^{th}-7^{th} millennium BC, Berger et al., 2020). However, OSL ages obtained for the top of the sequence are likely underestimated, since two out of three ages obtained are younger than 300 years, indicating a recent resetting of the OSL signal corresponding to reworked sediments. Ages obtained for the intermediate phases VII and VIII suggest an occupation time spanning from ca. 6000 to 5000 years BP (~4000-3000 years BC). Chronological data obtained on the sediment from the Khor al Jaramah cores indicate that the formation of the lagoon/mangrove

occurred around ~5900-4700 years ago (3900-2600 years BC), coinciding with the Neolithic occupation at the shell midden.

Acknowledgments

This study is part of the NeoArabia project (Dir. J.F. Berger), funded by the French National Research Agency (ANR-16-CE03-0007), dealing with the very long span of the Arabian Neolithic (6200-2800 BC). We thank all the team members of NeoArabia for their help in the field and for discussing the data.

We thank the Ministry of Heritage and Culture of the Sultanate of Oman for granting permission for fieldwork along the Omani Arabian sea shores, with specific reference to H.E. Salim Mohammed Almahruqi, Undersecretary for Heritage; Mr Sultan Said Al-Bakri, Director General for Archaeology; Mr Khamis Al-Asmi, Director of the Department of Excavations and Archaeological Studies.

V. Charpentier would like to thank the Consultative Commission for Excavations Abroad of the Ministry of European and Foreign Affairs, for granting the French Archaeological Mission.

M. Richard and N. Mercier are grateful to LaScArBx (Bordeaux Archaeological Sciences Labex) administrated by ANR (Agence Nationale de la Recherche) with the reference ANR-10-LABX-52.

We thank the two anonymous reviewers for their constructive remarks on this manuscript.

References

Arnold, L.J., Demuro, M., Ruiz, M.N., 2012. Empirical insights into multi-grain averaging effects from 'pseudo' single-grain OSL measurements, Radiation Measurements 47, 652-658.

Bassinot, F.C., Marzin, C., Braconnot, P., Marti, O., Mathien-Blard, E., Lombard, F., Bopp, L., 2011. Holocene evolution of summer winds and marine productivity in the tropical Indian Ocean in response to insolation forcing: data-model comparison, Climate of the Past 7, 815-829.

Berger, J.-F., Davtian, G., Cleuziou, S., 2005. Évolution paléogéographique du Ja'alan (Oman) à l'Holocène moyen : impact sur l'évolution des paléomilieux littoraux et les stratégies d'adaptation des communautés humaines. Paléorient 31, 46-63.

Berger, J.F., Charpentier, V., Crassard, R., Martin, C., Davtian, G., López-Sáez, J.A., 2013. The dynamics of mangrove ecosystems, changes in sea level and the strategies of Neolithic settlements along the coast of Oman (6000–3000 cal. BC). Journal of Archaeological Science 40, 3087-3104.

Berger, J.F., Guilbert-Berger, R., Marast, A., Munoz, O., Guy, H., Barra, A., López-Sáez, J.A., Pérez-Díaz, S., Mashkour, M., Debue, K., Lefèvre, C., Gosselin, M., Brugnaux, G., Mougne, C., Thorin, S., Nisbet, R., Oberlin, C., Mercier, N., Richard, M., Depreux, B., Bearez, P., 2020. First contribution of the excavation and the chronostratigraphic study of Ruways 1 Neolithic shell midden (Oman), in terms of Neolithization, palaeoeconomy, social-environmental interactions and site formation processes, Arabian Archaeology and Epigraphy, 32-49.

Brennan, B.J., Lyons, R.G., Phillips, S.W., 1991. Attenuation of alpha particle track dose for spherical grains. International Journal of Radiation Applications and Instrumentation. Part D. Nuclear Tracks and Radiation Measurements 18, 249-253.

Buylaert, J.-P., Thiel, C., Murray, A., Vandenberghe, D., Yi, S., Lu, H., 2011. IRSL and post-IR IRSL residual doses recorded in modern dust samples from the Chinese Loess Plateau. 38, 432.

Charpentier, V., Marquis, P., Pellé, É., 2003. La nécropole et les derniers horizons Ve millénaire du site de Gorbat al-Mahar (Suwayh, SWY-1, Sultanat d'Oman) : premiers résultats. Proceedings of the Seminar for Arabian Studies 33, 11-19.

Charpentier, V., 2008. Hunter-gathers of the “empty quarter of the early Holocene” to the last Neolithic societies: chronology of the late prehistory off South-Eastern Arabia (8000-3100 BC). Proceedings of the Seminar for Arabian Studies 38, 59-82.

Charpentier, V. Lacaze, M. Marquis, P. Marrast, A. Mashkour, M. Munoz, O. , E. Pellé (Forthcoming). First Neolithic communities in the Arabian Sea. The excavation of the 6th-5th millennium BCE Suwayh 1 settlement, (Sultanate of Oman). Arabian Archaeology and Epigraphy.

Crassard, R., Drechsler, P., 2013. Towards new paradigms: multiple pathways for the Arabian Neolithic, Arabian Archaeology and Epigraphy 24, 3-8.

Duller, G.A., 2007. Assessing the error on equivalent dose estimates derived from single aliquot regenerative dose measurements. Ancient TL 25, 15-24.

506 Duller, G.A., Bøtter-Jensen, L., Murray, A.S., 2000. Optical dating of single sand-sized grains
507 of quartz: sources of variability, Radiation Measurements 32, 453-457.
508 Fleitmann, D., Burns, S.J., Mangini, A., Mudelsee, M., Kramers, J., Villa, I., Neff, U., Al-
509 Subbary, A.A., Buettner, A., Hippler, D., Matter, A., 2007. Holocene ITCZ and Indian
510 monsoon dynamics recorded in stalagmites from Oman and Yemen (Socotra),
511 Quaternary Science Reviews 26, 170-188.
512 Galbraith, R.F., Green, P.F., 1990. Estimating the component ages in a finite mixture.
513 International Journal of Radiation Applications and Instrumentation. Part D. Nuclear
514 Tracks and Radiation Measurements 17, 197-206.
515 Galbraith, R.F., Roberts, R.G., Laslett, G.M., Yoshida, H., Olley, J.M., 1999. Optical dating
516 of single and multiple grains of quartz from Jinmium rock shelter, northern Australia:
517 Part I, experimental design and statistical models. Archaeometry 41, 339-364.
518 Galbraith, R.F., Roberts, R.G., 2012. Statistical aspects of equivalent dose and error
519 calculation and display in OSL dating: An overview and some recommendations,
520 Quaternary Geochronology 11, 1-27.
521 Guérin, G., Mercier, N., Adamiec, G., 2011. Dose-rate conversion factors: update. Ancient TL
522 29, 5-8.
523 Guérin, G., Mercier, N., Nathan, R., Adamiec, G., Lefrais, Y., 2012. On the use of the infinite
524 matrix assumption and associated concepts: A critical review. Radiation Measurements
525 47, 778-785.
526 Jung, S.J.A., Davies, G.R., Ganssen, G.M., Kroon, D., 2004. Synchronous Holocene sea
527 surface temperature and rainfall variations in the Asian monsoon system, Quaternary
528 Science Reviews 23, 2207-2218.
529 Lézine, A.-M., Saliège, J.-F., Mathieu, R., Tagliatela, T.-L., Mery, S., Charpentier, V.,
530 Cleuziou, S., 2002. Mangroves of Oman during the late Holocene; climatic implications
531 and impact on human settlements. Vegetation History and Archaeobotany 11, 221-232.
532 Lézine, A.-M., Robert, C., Cleuziou, S., Inizan, M.-L., Braemer, F., Saliège, J.-F., Sylvestre,
533 F., Tiercelin, J.-J., Crassard, R., Méry, S., Charpentier, V., Steimer-Herbet, T., 2010.
534 Climate change and human occupation in the Southern Arabian lowlands during the last
535 deglaciation and the Holocene, Global and Planetary Change 72, 412-428.
536 Marrast, A., Béarez, P., Charpentier, V., 2020. Sharks in the lagoon? Fishing exploitation at
537 the Neolithic site of Suwayh 1 (Ash Sharqiyah region, Arabian Sea, Sultanate of Oman),
538 Arabian Archaeology and Epigraphy 31, 178-193.

539 Martin, C., 2005. Stratégies et statut de la collecte des mollusques marins sur les sites côtiers
540 d'Oman du Néolithique à l'âge du Bronze: Apport des sites de suwayh 1, ra's al-
541 Khabbah 1 et Ra's al-Jinz 2, Paléorient, 169-175.
542 Mercier, N., Falguères, C., 2007. Field gamma dose-rate measurement with a NaI(Tl)
543 detector: re-evaluation of the "threshold" technique. Ancient TL 25, 1-4.
544 Murray, A.S., Wintle, A.G., 2000. Luminescence dating of quartz using an improved single-
545 aliquot regenerative-dose protocol. Radiation Measurements 32, 57-73.
546 Parker, A.G., Rose, J.I., 2008. Climate change and human origins in southern Arabia,
547 Proceedings of the Seminar for Arabian Studies 38, 25-42.
548 Prescott, J.R., Hutton, J.T., 1988. Cosmic ray and gamma ray dosimetry for TL and ESR.
549 International Journal of Radiation Applications and Instrumentation. Part D. Nuclear
550 Tracks and Radiation Measurements 14, 223-227.
551 Preusser, F., Schmitt, L., Delile, H., Grosprêtre, L., 2011. Optically Stimulated Luminescence
552 (OSL) dating of the sedimentation history of the Yzeron Basin (Chaudanne sub-
553 catchment), Rhône Valley, France, Quaternaire 22, 73-83.
554 Richter, D., Richter, A., Dornich, K., 2013. Lexsyg — A new system for luminescence
555 research. Geochronometria 40, 220-228.
556 Richter, D., Richter, A., Dornich, K., 2015. Lexsyg smart - a luminescence detection system
557 for dosimetry, material research and dating application. Geochronometria 42, 202-209.
558 Thomsen, K.J., Murray, A.S., Jain, M., Bøtter-Jensen, L., 2008. Laboratory fading rates of
559 various luminescence signals from feldspar-rich sediment extracts. Radiation
560 Measurements 43, 1474-1486.
561
562
563
564 **Figures**
565
566 Fig. 1: Location of shell middens (Ruways 1 and Suwayh 1, red squares) and cores (Ruways,
567 Daffah and Khor al Jaramah, red circles) in the eastern coast of the Sultanate of Oman.
568 Modified after Berger et al. (2005: Figure 2).
569
570 Fig. 2: Ruways 1. Stratigraphic profile (east-west) and depositional phases.
571

572 Fig. 3: Suwayh 1. Stratigraphic profile. Drawing by J-F. Berger and G. Davtian. After
573 Charpentier (2008: Figure 3).
574
575 Fig. 4: Shine-down OSL curve (signal versus stimulation time) of BDX 19226.
576
577 Fig. 5: Ruways 1. a. Abanico plots of equivalent doses obtained for BDX 19226 (a), 19227
578 (b) and 19228 (c) (Phase II). Overdispersion values are 23 ± 3% (a), 35 ± 4% (b) and 32 ± 4%
579 (c) respectively.
580
581 Fig. 6: Graphic comparison of D_e values obtained using the FMM and CAM. Samples number
582 follows the stratigraphic order (depth and layer attribution from Tabs. 1 and 6). For D_e values
583 < 1 Gy, error bars are not visible due to the scale. For BDX 19234, the FMM and CAM D_e
584 values are indistinguishable.
585
586 Fig. 7: Suwayh 1: Histogram of equivalent doses obtained for BDX 19238 (a), 19239 (b) and
587 19240 (c). Overdispersion values are 20 ± 2% (a), 13 ± 2% (b) and 20 ± 2% (c).
588
589 Fig. 8: Dose rate distribution (%).
590
591 Fig. 9: Graphic representation of luminescence ages obtained as a function of depth. For
592 young ages (< 1 ka), error bars are not visible due to the scale. The samples that fall within
593 the grey shade can be correlated: the formation of the lagoon in Khor al Jaramah is
594 contemporaneous with human occupation at Ruways 1 (phases VII/VIII) and Suwayh 1.

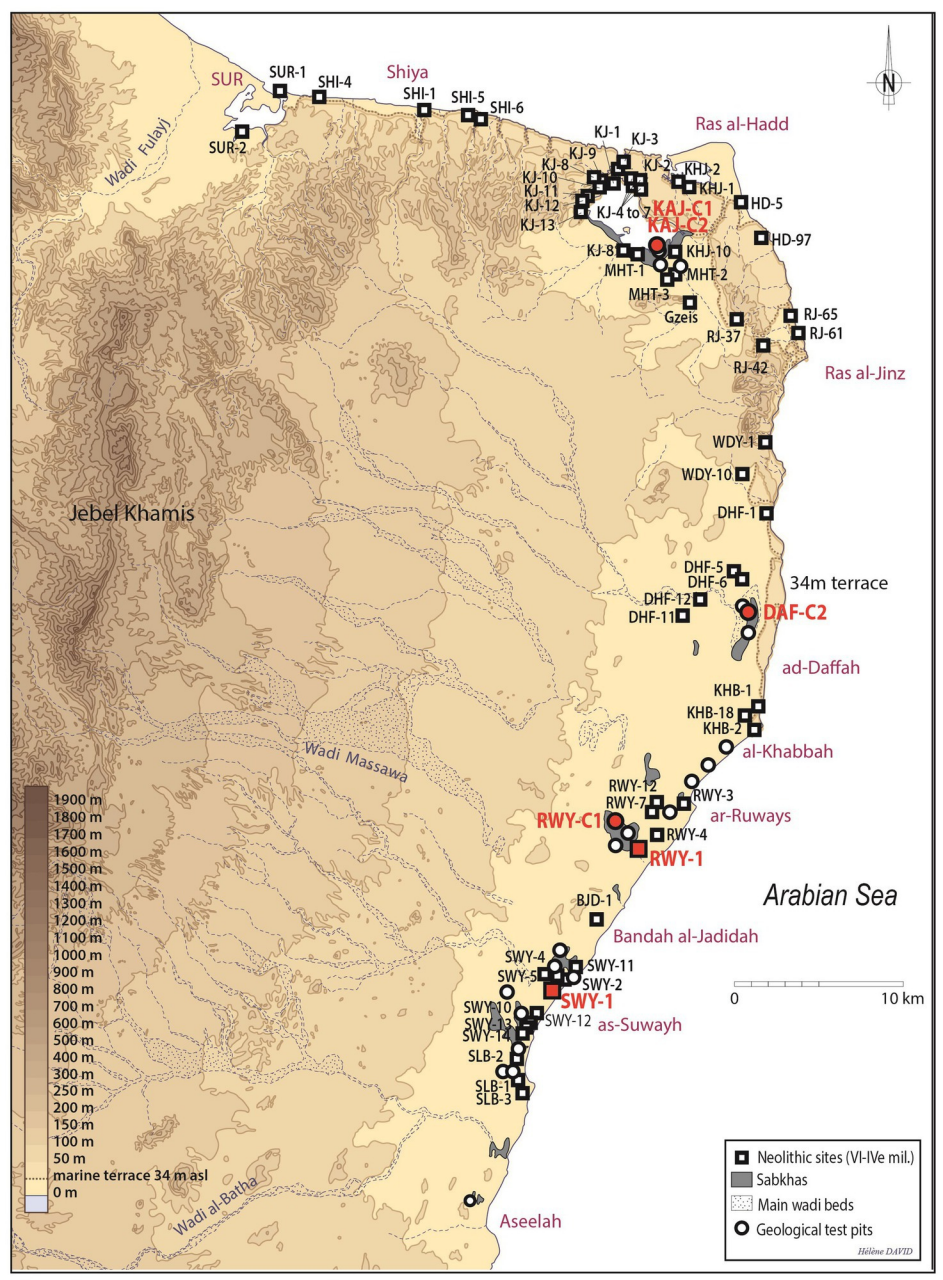
SUR
SUR-1
SHI-4
SUR-2
Shiya
SHI-1
SHI-5
SHI-6
Wadi Fulayj
KJ-1
KJ-3
KJ-9
KJ-2
KHJ-2
KJ-8
KJ-10
KJ-11
KJ-12
KJ-13
KJ-4 to 7
KAJ-C1
KAJ-C2
KHJ-1
HD-5
HD-97
KJ-8
KHJ-10
MHT-1
MHT-2
MHT-3
Gzeis
RJ-65
RJ-61
RJ-37
RJ-42
Ras al-Hadd
Ras al-Jinz
WDY-1
WDY-10
Jebel Khamis
DHF-1
DHF-5
DHF-6
DHF-12
DHF-11
34m terrace
DAF-C2
ad-Daffah
KHB-1
KHB-18
KHB-2
al-Khabbah
Wadi Massawa
RWY-12
RWY-7
RWY-3
RWY-C1
ar-Ruways
RWY-4
RWY-1
Arabian Sea
BJD-1
Bandah al-Jadidah
SWY-4
SWY-11
SWY-5
SWY-2
SWY-1
SWY-10
SWY-13
SWY-14
SWY-12
as-Suwayh
SLB-2
SLB-1
SLB-3
0
10 km
1900 m
1800 m
1700 m
1600 m
1500 m
1400 m
1300 m
1200 m
1100 m
1000 m
900 m
800 m
700 m
600 m
500 m
400 m
300 m
250 m
200 m
150 m
100 m
50 m
marine terrace 34 m asl
0 m
Wadi al-Batha
Aseelah
Neolithic sites (VI-IVe mil.)
Sabkhas
Main wadi beds
Geological test pits
Hélène DAVID

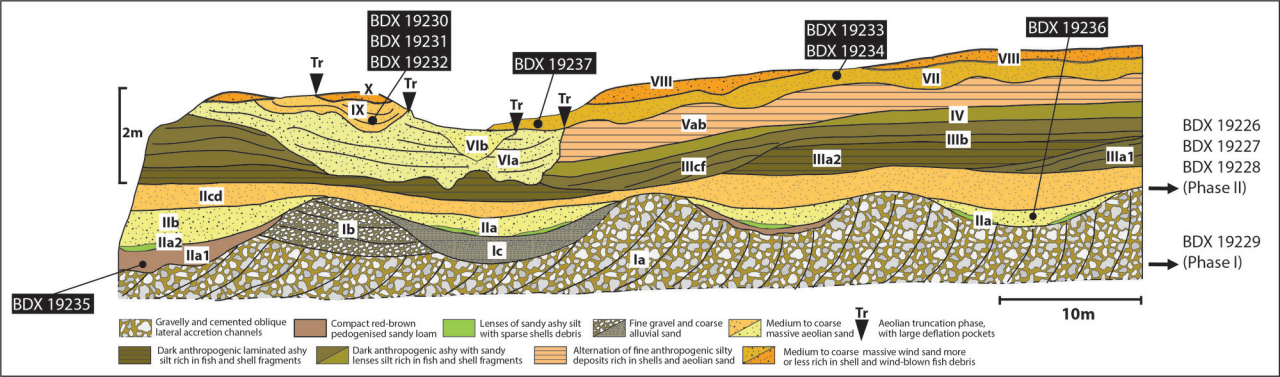
BDX 19230
BDX 19231
BDX 19232
BDX 19237
BDX 19233
BDX 19234
BDX 19236
Tr
X
IX
VIII
VII
2m
VIb
VIa
Vab
IV
IIIb
IIIcf
IIIa2
IIIa1
BDX 19226
BDX 19227
BDX 19228
(Phase II)
IIcd
IIb
IIa2
IIa1
Ib
IIa
Ic
Ia
BDX 19229
(Phase I)
BDX 19235
10m
Gravelly and cemented oblique lateral accretion channels
Compact red-brown pedogenised sandy loam
Lenses of sandy ashy silt with sparse shells debris
Fine gravel and coarse alluvial sand
Medium to coarse massive aeolian sand
Aeolian truncation phase, with large deflation pockets
Dark anthropogenic laminated ashy silt rich in fish and shell fragments
Dark anthropogenic ashy with sandy lenses silt rich in fish and shell fragments
Alternation of fine anthropogenic silty deposits rich in shells and aeolian sand
Medium to coarse massive wind sand more or less rich in shell and wind-blown fish debris

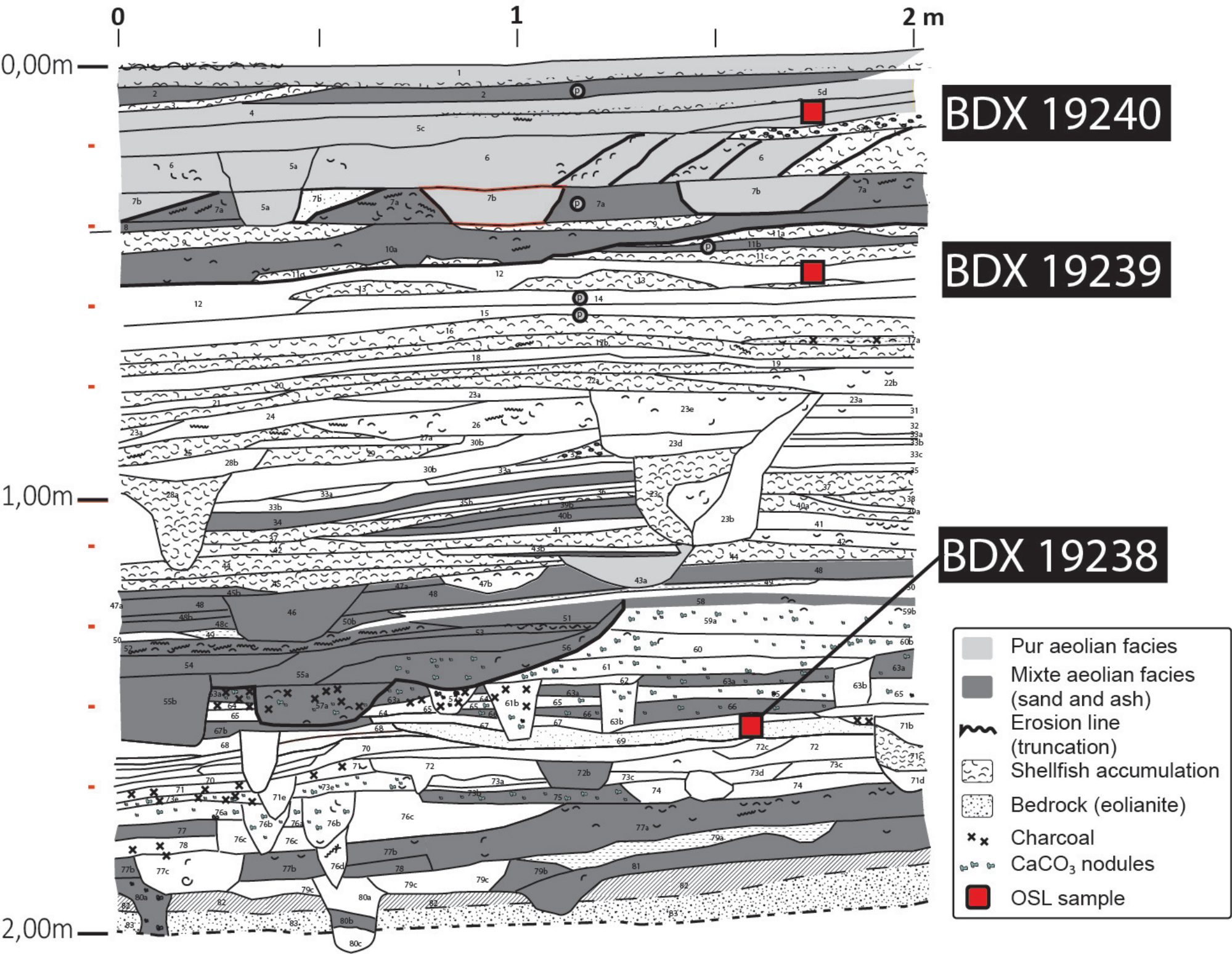
0
1
2 m
0,00m
1,00m
2,00m
BDX 19240
BDX 19239
BDX 19238
Pur aeolian facies
Mixte aeolian facies (sand and ash)
Erosion line (truncation)
Shellfish accumulation
Bedrock (eolianite)
Charcoal
$CaCO_3$ nodules
OSL sample

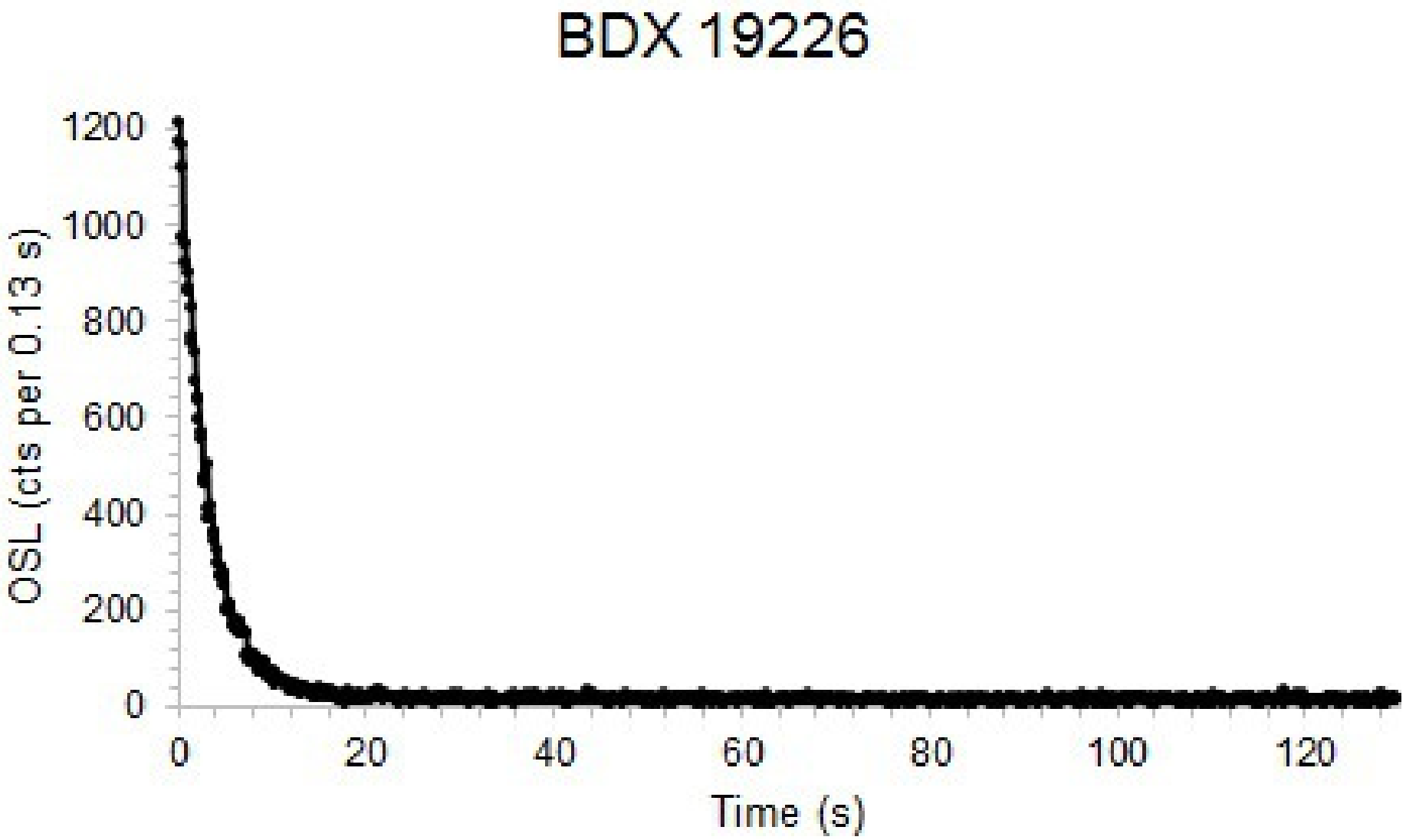
BDX 19226
OSL (cts per 0.13 s)
1200
1000
800
600
400
200
0
0
20
40
60
80
100
120
Time (s)

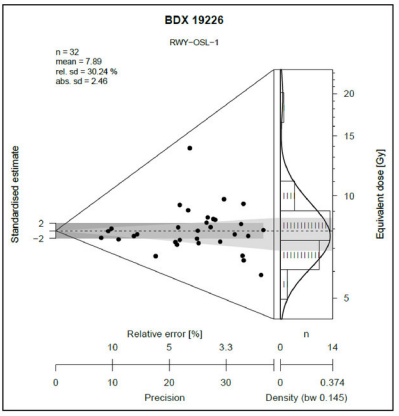
BDX 19226
RWY-OSL-1
n = 32
mean = 7.89
rel. sd = 30.24 %
abs. sd = 2.46
Standardised estimate
Equivalent dose [Gy]
Relative error [%]
n
Precision
Density (bw 0.145)

a.

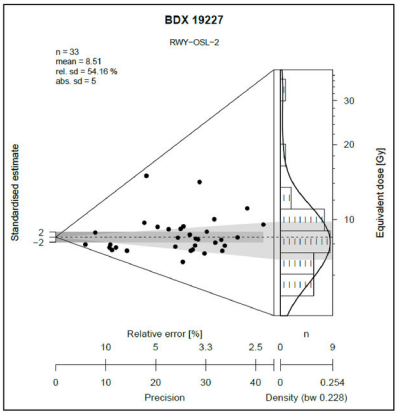
BDX 19227
RWY-OSL-2
n = 33
mean = 8.51
rel. sd = 54.16 %
abs. sd = 5
Standardised estimate
Equivalent dose [Gy]
Relative error [%]
n
Precision
Density (bw 0.228)

b.

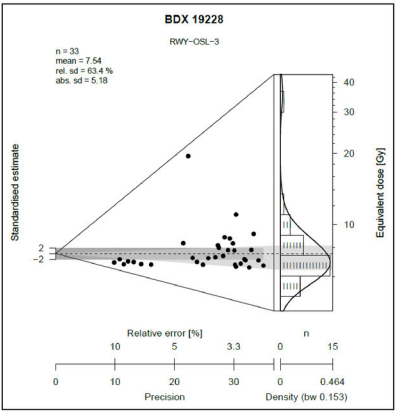
BDX 19228
RWY-OSL-3
n = 33
mean = 7.54
rel. sd = 63.4 %
abs. sd = 5.18
Standardised estimate
Equivalent dose [Gy]
Relative error [%]
n
Precision
Density (bw 0.153)

c.

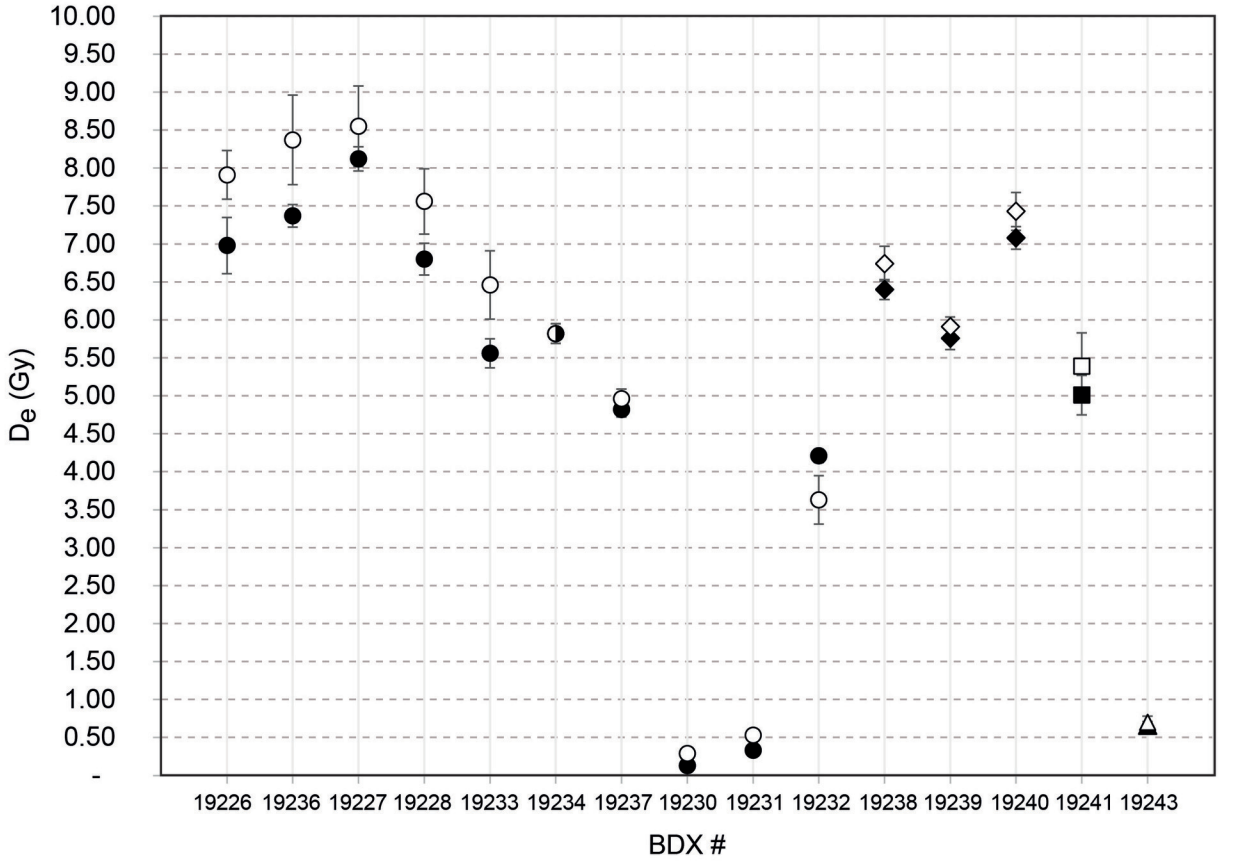
10.00
9.50
9.00
8.50
8.00
7.50
7.00
6.50
6.00
5.50
5.00
4.50
4.00
3.50
3.00
2.50
2.00
1.50
1.00
0.50
-
De (Gy)
19226 19236 19227 19228 19233 19234 19237 19230 19231 19232 19238 19239 19240 19241 19243
BDX #
Ruways 1 (FMM)
Suwayh 1 (FMM)
Ruways-core 1 (FMM)
Daffah-Core 2 (FMM)
Ruways-1 (CAM)
Suwayh 1 (CAM)
Ruways-core 1 (CAM)
Daffah-Core 2 (CAM)

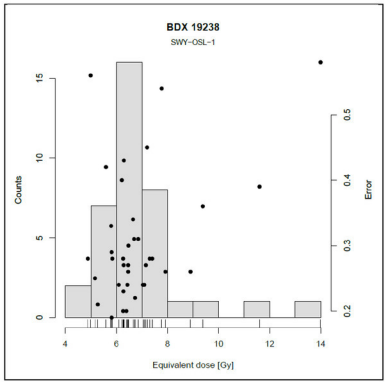
BDX 19238
SWY-OSL-1
Counts
Error
Equivalent dose [Gy]

a.

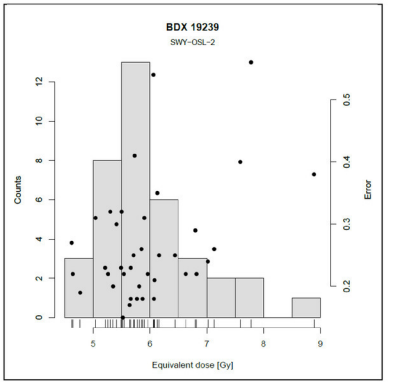
BDX 19239
SWY-OSL-2
Counts
Error
Equivalent dose [Gy]

b.

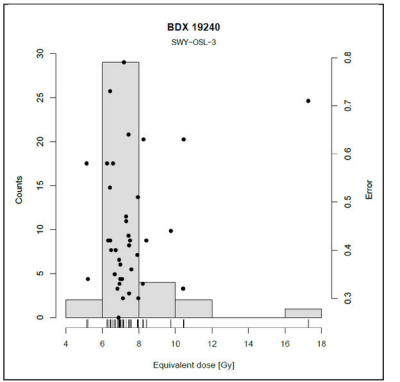
BDX 19240
SWY-OSL-3
Counts
Error
Equivalent dose [Gy]

c.

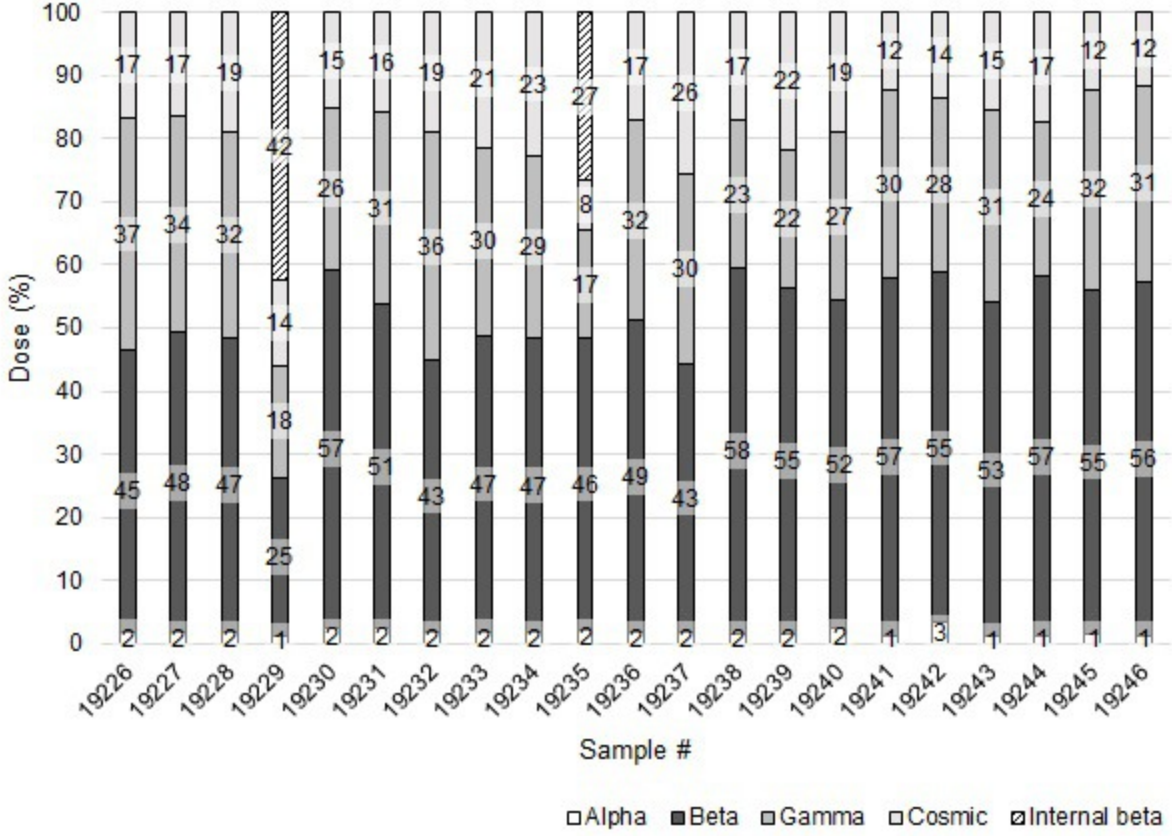
Dose (%)
100
90
80
70
60
50
40
30
20
10
0
19226 19227 19228 19229 19230 19231 19232 19233 19234 19235 19236 19237 19238 19239 19240 19241 19242 19243 19244 19245 19246
Sample #
Alpha
Beta
Gamma
Cosmic
Internal beta

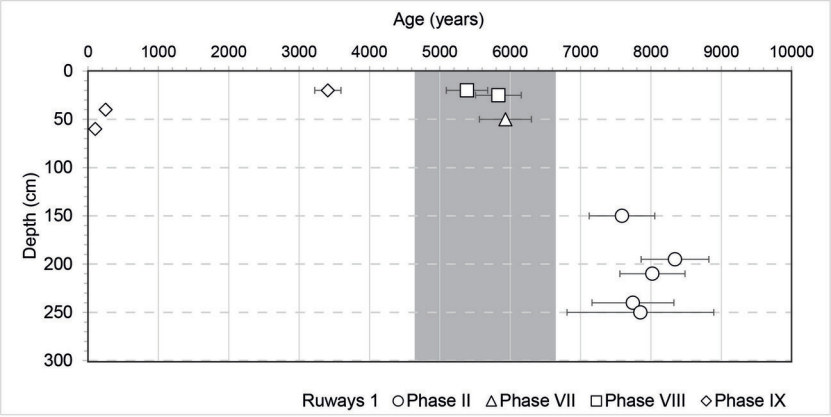
Age (years)
0 1000 2000 3000 4000 5000 6000 7000 8000 9000 10000
Depth (cm)
0 50 100 150 200 250 300
Ruways 1 ○Phase II △Phase VII □Phase VIII ◇Phase IX

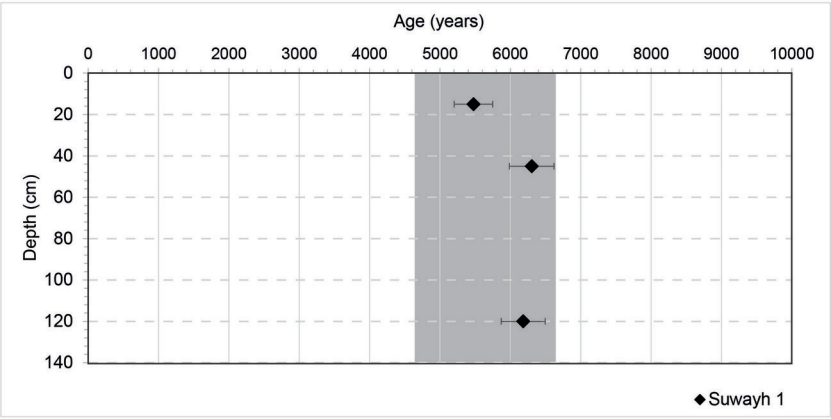
Age (years)
0 1000 2000 3000 4000 5000 6000 7000 8000 9000 10000
Depth (cm)
0 20 40 60 80 100 120 140
◆Suwayh 1

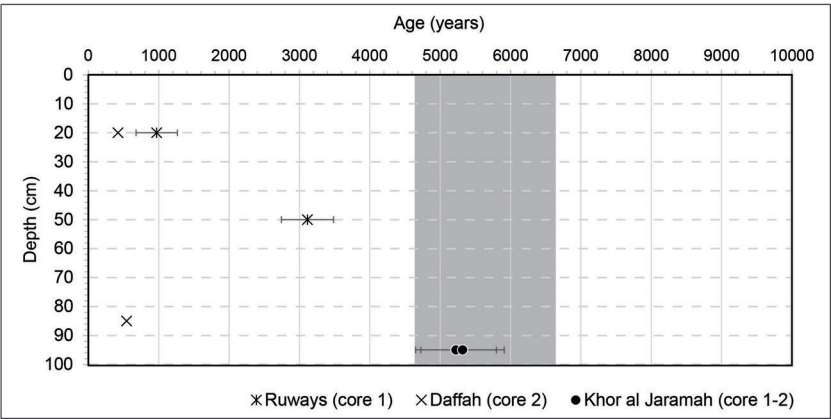
Age (years)
0 1000 2000 3000 4000 5000 6000 7000 8000 9000 10000
Depth (cm)
0 10 20 30 40 50 60 70 80 90 100
✳Ruways (core 1) ×Daffah (core 2) ●Khor al Jaramah (core 1-2)

Lab #	Site	Sample #	Depth (cm)	Context	Sample type	Sedimentology	Material[a]	Granulometric fraction
19226	Ruways 1	RWY-1-OSL-1	240	Section	Tube	Fine sand	Q	160-200
19227	Ruways 1	RWY-1-OSL-2	195	Section	Tube	Fine sand	Q	160-200
19228	Ruways 1	RWY-1-OSL-3	150	Section	Tube	Fine sand	Q	160-200
19229	Ruways 1	RWY-1-OSL-4	195	Section	Bag	Sand	F	160-200
19230	Ruways 1	RWY-1-OSL-5	60	Section	Bag	Sandy lens	Q	160-200
19231	Ruways 1	RWY-1-OSL-6	40	Section	Bag	Sandy lens	Q	160-200
19232	Ruways 1	RWY-1-OSL-7	20	Section	Bag	Sandy lens	Q	160-200
19233	Ruways 1	RWY-1-OSL-8	50	Section	Bag	Sand	Q	160-200
19234	Ruways 1	RWY-1-OSL-9	25	Section	Bag	Sand	Q	160-200
19235	Ruways 1	RWY-1-OSL-10	250	Section	Bag	Sand	F	160-200
19236	Ruways 1	RWY-1-OSL-11	210	Section	Bag	Sand	Q	160-200
19237[b]	Ruways 1	RWY-1-OSL-12	20	Section	Bag	Sand	Q	120-160
19238	Suwayh 1	SWY-OSL-1	120	Section	Bag	Silt	Q	120-160
19239	Suwayh 1	SWY-OSL-2	45	Section	Bag	Silt	Q	120-160
19240	Suwayh 1	SWY-OSL-3	15	Section	Bag	Silt	Q	120-160
19241	Ruways-C1	RWY-C1-OSL-1	50	Core	Tube	Silt	Q	100-120
19242	Ruways-C1	RWY-C1-OSL-2	20	Core	Tube	Coarse sand	Q	100-120
19243	Daffah-C2	DAF-C2-OSL-1	85	Core	Tube	Silt	Q	120-160
19244	Daffah-C2	DAF-C2-OSL-2	20	Core	Tube	Silt	Q	100-120
19245[b]	Khor al Jaramah-C1	KAJ-C1-OSL-1	90-100	Core	Tube	Silt	Q	100-120
19246[b]	Khor al Jaramah-C2	KAJ-C2-OSL-1	90-100	Core	Tube	Clayey-silt	Q	100-120

Tab. 1. List of samples analysed in this study. Sample numbers match those provided in SOM.

[a] Material: quartz (Q) / feldspars (F)

[b] no in-situ gamma dosimetry measurements were performed for these samples (see text).

Step	Treatment
1	Given dose
2	Preheat (190-260°C for 10 s)
3	IR stimulation for 60 s at 50°C
4 (L_x)	Green stimulation for 100 s at 125°C
5	Given test dose
6	Cutheat (160-200°C for 0 s)
7	IR stimulation for 60 s at 50°C
8 (T_x)	Green stimulation for 100 s at 125°C
9	Return to 1

Tab. 2. OSL SAR measurement protocol applied to quartz.

Step	Treatment
1	Given dose
2	Preheat (250°C for 60 s)
3	IR stimulation for 200 s at 50°C
4 (L_x)	IRSL stimulation for 200 s at 225°C
5	Given test dose
6	Preheat (250°C for 60 s)
7	IR stimulation for 200 s at 50°C
8 (T_x)	IRSL stimulation for 200 s at 225°C
9	IRSL stimulation for 60 s at 325°C
10	Return to 1

Tab. 3. $pIRIR_{225}$ SAR measurement protocol applied to feldspars.

Lab #	Site	*n* aliquots	DRT	Dose (Gy)
19226	Ruways 1	3	1.00 ± 0.03	5.4
19227	Ruways 1	3	1.00 ± 0.06	5.4
19228	Ruways 1	3	0.99 ± 0.08	5.4
19230	Ruways 1	3	1.04 ± 0.05	0.9
19231	Ruways 1	3	1.01 ± 0.01	0.9
19232	Ruways 1	3	0.96 ± 0.02	5.4
19233	Ruways 1	3	0.98 ± 0.06	5.4
19234	Ruways 1	3	1.00 ± 0.03	5.4
19236	Ruways 1	3	0.99 ± 0.02	5.4
19237	Ruways 1	3	0.96 ± 0.03	5.4
19238	Suwayh 1	5	0.99 ± 0.02	5.3
19239	Suwayh 1	5	0.99 ± 0.03	5.3
19240	Suwayh 1	4	1.02 ± 0.02	5.3
19241	Ruways-C1	5	0.97 ± 0.07	3.5
19242	Ruways-C1	5	1.08 ± 0.23	1.8
19243	Daffah-C2	5	1.44 ± 0.16	0.5
19244	Daffah-C2	5	1.25 ± 0.19	0.5
19245	Khor al Jaramah-C1	5	0.89 ± 0.06	7.1
19246	Khor al Jaramah-C2	5	0.92 ± 0.03	7.1

Tab. 4. Dose recovery test results obtained on quartz. The dose (Gy) is the artificial dose applied after bleaching the samples in a solar simulator (see text).

Lab #	Site	^{238}U (ppm)	^{232}Th (ppm)	K (%)	Water content (weight%)
19226	Ruways 1	2.36 ± 0.02	0.57 ± 0.02	0.16 ± 0.01	3
19227	Ruways 1	2.25 ± 0.02	0.83 ± 0.02	0.25 ± 0.01	3
19228	Ruways 1	2.25 ± 0.02	0.60 ± 0.02	0.19 ± 0.01	3
19229	Ruways 1	0.53 ± 0.01	1.12 ± 0.01	0.30 ± 0.01	3
19230	Ruways 1	3.16 ± 0.04	4.18 ± 0.04	0.36 ± 0.01	3
19231	Ruways 1	3.20 ± 0.04	4.62 ± 0.04	0.28 ± 0.01	3
19232[a]	Ruways 1	2.42 ± 0.02	2.65 ± 0.02	0.27 ± 0.01	3
19233	Ruways 1	2.36 ± 0.03	0.88 ± 0.03	0.20 ± 0.01	3
19234	Ruways 1	2.31 ± 0.03	0.92 ± 0.03	0.24 ± 0.01	3
19235	Ruways 1	1.57 ± 0.02	3.91 ± 0.02	0.85 ± 0.01	3
19236	Ruways 1	2.19 ± 0.02	0.86 ± 0.02	0.25 ± 0.01	3
19237[a]	Ruways 1	1.55 ± 0.02	1.11 ± 0.02	0.25 ± 0.01	3
19238	Suwayh 1	1.28 ± 0.02	1.91 ± 0.02	0.62 ± 0.01	9
19239	Suwayh 1	1.18 ± 0.02	1.79 ± 0.02	0.51 ± 0.01	9
19240	Suwayh 1	2.67 ± 0.02	3.28 ± 0.02	0.44 ± 0.01	9
19241	Ruways-C1	1.46 ± 0.02	3.14 ± 0.02	1.15 ± 0.01	19
19242	Ruways-C1	4.07 ± 0.04	6.46 ± 0.04	0.56 ± 0.01	12
19243	Daffah-C2	1.20 ± 0.03	1.50 ± 0.03	0.80 ± 0.01	17
19244	Daffah-C2	1.18 ± 0.01	2.06 ± 0.01	0.92 ± 0.01	13
19245[a]	Khor al Jaramah-C1	1.07 ± 0.03	4.34 ± 0.03	1.02 ± 0.01	17
19246[a]	Khor al Jaramah-C2	1.13 ± 0.02	4.48 ± 0.05	1.26 ± 0.02	27

Tab. 5. Radioisotopes content measured in the sediment samples using BEGe gamma-ray spectrometry and water content used for age calculation.

[a] no in-situ gamma dosimetry measurements were performed for these samples. The gamma dose rates were derived using U, Th and K content.

Lab #	Site	*n*	Dose rate (µGy.a^{-1})						D_e FMM	Age FMM	D_e CAM	Age CAM	Age
			Alpha	Beta	Gamma	Cosmic	Internal	Total	(Gy)	(years)	(Gy)	(years)	(years BC)
19226 (Q)	Ruways 1 (Phase II)	32	16 ± 3	404 ± 4	329 ± 16	152 ± 10		901 ± 17	6.98 ± 0.37	**7 740 ± 580**	7.91 ± 0.32	8 780 ± 590	5 730 ± 580
19227 (Q)	Ruways 1 (Phase II)	33	16 ± 3	463 ± 5	333 ± 17	161 ± 10		973 ± 18	8.12 ± 0.16	**8 340 ± 480**	8.55 ± 0.53	8 780 ± 720	6 320 ± 480
19228 (Q)	Ruways 1 (Phase II)	33	16 ± 3	418 ± 5	291 ± 15	171 ± 10		896 ± 16	6.80 ± 0.21	**7 590 ± 470**	7.56 ± 0.43	8 440 ± 650	5 570 ± 470
19229 (F)	Ruways 1 (Phase I)	8	14 ± 2	298 ± 5	210 ± 10	161 ± 20	500 ± 50	1183 ± 51	-	-	520.66 ± 79.78	**440 000 ± 76 000**	438 000 ± 76 000
19230 (Q)	Ruways 1 (Phase IX)	33	30 ± 5	721 ± 10	325 ± 16	194 ± 10		1271 ± 19	0.13 ± 0.01	**100 ± 10**	0.29 ± 0.05	230 ± 40	-
19231 (Q)	Ruways 1 (Phase IX)	38	32 ± 5	677 ± 9	405 ± 20	207 ± 10		1321 ± 23	0.33 ± 0.01	**250 ± 20**	0.53 ± 0.08	400 ± 60	-
19232 (Q)*	Ruways 1 (Phase IX)	40	22 ± 3	533 ± 5	444 ± 3	236 ± 10		1235 ± 7	4.21 ± 0.09	**3 410 ± 190**	3.63 ± 0.32	2 940 ± 290	1 390 ± 190
19233 (Q)	Ruways 1 (Phase VII)	24	17 ± 3	440 ± 8	280 ± 14	200 ± 10		937 ± 16	5.56 ± 0.19	**5 930 ± 370**	6.46 ± 0.45	6 890 ± 590	3 910 ± 370
19234 (Q)	Ruways 1 (Phase VIII)	22	17 ± 3	465 ± 10	289 ± 14	227 ± 10		998 ± 17	5.82 ± 0.13	5 830 ± 330	5.82 ± 0.12	**5 830 ± 320**	3 810 ± 320
19235 (F)	Ruways 1 (Phase II)	5	43 ± 8	866 ± 9	323 ± 16	150 ± 20	500 ± 50	1882 ± 54	-	-	14.78 ± 1.55	**7 850 ± 1 040**	5 830 ± 1 040
19236 (Q)	Ruways 1 (Phase II)	37	16 ± 3	454 ± 6	291 ± 15	158 ± 10		919 ± 16	7.37 ± 0.15	**8 020 ± 460**	8.37 ± 0.59	9 110 ± 800	6 000 ± 460
19237 (Q)*	Ruways 1 (Phase VIII)	27	17 ± 3	392 ± 4	276 ± 2	236 ± 10		921 ± 5	4.82 ± 0.1	5 230 ± 270	4.96 ± 0.13	**5 390 ± 290**	3 370 ± 290
19238 (Q)	Suwayh 1	37	16 ± 2	600 ± 7	241 ± 12	178 ± 10		1035 ± 14	6.40 ± 0.13	**6 180 ± 310**	6.74 ± 0.23	6 510 ± 370	4 160 ± 310
19239 (Q)	Suwayh 1	38	14 ± 2	513 ± 8	207 ± 10	203 ± 10		937 ± 13	5.76 ± 0.15	6 140 ± 320	5.91 ± 0.13	**6 300 ± 320**	4 290 ± 320
19240 (Q)	Suwayh 1	38	31 ± 5	672 ± 6	345 ± 17	246 ± 10		1293 ± 19	7.08 ± 0.15	**5 480 ± 270**	7.43 ± 0.25	5 750 ± 320	3 460 ± 270
19241 (Q)	Ruways-C1	24	21 ± 3	913 ± 9	475 ± 24	200 ± 10		1609 ± 26	5.01 ± 0.26	**3 110 ± 370**	5.39 ± 0.44	3 350 ± 450	1 100 ± 370
19242 (Q)	Ruways-C1	7	57 ± 8	959 ± 8	478 ± 24	236 ± 10		1730 ± 27	-	-	1.68 ± 0.51	**970 ± 290**	-
19243 (Q)	Daffah-C2	22	13 ± 2	643 ± 13	372 ± 19	187 ± 10		1214 ± 23	0.66 ± 0.05	**540 ± 70**	0.70 ± 0.08	580 ± 90	-
19244 (Q)	Daffah-C2	14	17 ± 2	769 ± 8	331 ± 17	236 ± 10		1352 ± 19	-	-	0.57 ± 0.06	**420 ± 50**	-
19245 (Q)*	Khor al Jaramah-C1	9	22 ± 3	829 ± 15	481 ± 6	184 ± 10		1516 ± 16	-	-	7.92 ± 0.42	**5 220 ± 570**	3 210 ± 570
19246 (Q)*	Khor al Jaramah-C2	7	20 ± 3	893 ± 9	494 ± 4	184 ± 10		1591 ± 10	-	-	8.46 ± 0.38	**5 320 ± 590**	3 300 ± 590

Tab. 6. OSL ages on quartz (Q) and $pIRIR_{225}$ ages on feldspar (F). Ages were rounded to ten years, except for BDX 19229, rounded to thousand years. The error on the age takes into account the systematic error. For samples with less than 22 aliquots measured, no FMM ages were calculated. CAM overdispersion values are presented in SOM Tab. S1 FMM components are provided in SOM Tab. S2. Age values used for interpretation are shown in bold text and are converted in years BC in the last column.
*no in-situ gamma dosimetry measurements were performed for these samples (see text).